Fermi National Accelerator Laboratory

FERMILAB-Conf-94/030-E

CDF

CDF End Plug Calorimeter Upgrade Project

Giorgio Apollinari

Rockefeller University
New York, New York 10021

Pawel de Barbaro

University of Rochester, Rochester, New York 14627
Fermi National Accelerator Laboratory, P.O. Box 500, Batavia, Illinois 60510

Masanori Mishina

National Laboratory for High Energy Physics, KEK
Tsukuba-shi Ibaraki-ken, Japan

January 1994

To be published in the proceedings of the *IV International Conference on the Calorimetry in High Energy Physics*, La Biodola, Elba, September 19-25, 1993

Disclaimer

CDF/PUB/CALORIMETER/CDFR/2432
FERMILAB-CONF-94/030-E

UR-1329
ER-40685-779

CDF END PLUG CALORIMETER UPGRADE PROJECT

Giorgio Apollinari
Rockefeller University, New York, NY 10021

Pawel de Barbaro
University of Rochester, Rochester, NY 14627

and
Masanori Mishina
National Laboratory for High Energy Physics, KEK
Tsukuba-shi Ibaraki-ken, Japan

Representing the CDF Plug Upgrade Group,
to be published in the proceedings of the IV International Conference on the Calorimetry in the High Energy Physics, La Biodola, Elba, Sep 19-25, 1993.

ABSTRACT

We report on the status of the CDF End Plug Upgrade Project. In this project, the CDF calorimeters in the end plug and the forward regions will be replaced by a single scintillator based calorimeter. After an extensive R&D effort on the tile/fiber calorimetry, we have now advanced to a construction phase. We review the results of the R&D leading to the final design of the calorimeters and the development of tooling devised for this project. The quality control program of the production of the electromagnetic and hadronic calorimeters is described. A shower maximum detector for the measurement of the shower centroid and the shower profile of electrons, γ and π^0 has been designed. Its performance requirements, R&D results and mechanical design are discussed.

1. Overview of the Project

1.1. Motivation

The **CDF** Collaboration has successfully completed Run Ia in August 1993, in which 21 pb^{-1} of data were recorded on tape. The Tevatron collider schedule is shown in Table 1. The next run, Run Ib, will start in December 1993 with the goal of accumulating 75 pb^{-1}. Following a fixed target run in 1995, the Tevatron will be switched back to the collider mode in 1996 (Run II) in which more than 200 pb^{-1} will be accumulated.

The number of proton and antiproton bunches in the Tevatron (6×6 through Run Ib) will be increased to 36×36 in Run II. This change will lead to an increase

in the luminosity, in part limited by the number of p and $\bar{p}$ in a single bunch. It will also result in a reduction of the probability of multiple interactions in a single bunch crossing.

Table 1. The Tevatron Collider Schedule

	88-89 Run	Run Ia 1992/93	Run Ib 1993/4	Run II 1996 (?)
Delivered Luminosity	9.6 pb^{-1}	30 pb^{-1}		
Integrated Luminosity	4 pb^{-1}	21 pb^{-1}	75 pb^{-1}	$\approx$ 200 pb^{-1}
Luminosity to tape	50%	70%		
Peak Luminosity $[cm^{-2}sec^{-1}]$	2×10^{30}	9.2×10^{30}	1.5×10^{31}	
Bunches	6 × 6	6 × 6	6 × 6	36 × 36
Interval	3.5 μsec	3.5 μsec	3.5 μsec	396 nsec

Table 2 shows the probability of two or more visible interactions in a single bunch crossing for various conditions of the beam luminosity and number of bunches. The peak luminosity in Run Ia reached $9.2 \times 10^{30} cm^{-2} sec^{-1}$ leading to the 60% probability of multiple interactions per bunch crossing. Following the upgrade to the injection linac energy from the original 200 MeV to 400 MeV, the luminosity in the upcoming Run Ib is expected to increase by 50% or more.

Table 2. Number of average events per single bunch crossing, assuming a visible cross-section of 44 mbarns. The probability of two or more events per bunch crossing is shown in brackets.

L $[cm^{-2}sec^{-1}]$	6 × 6	36 × 36	96 × 96
10^{30}	0.15 (7.5%)	0.017 (1.3%)	0.006 (0.5%)
10^{31}	1.50 (58.0%)	0.17 (12.3%)	0.058 (4.7%)
10^{32}		1.74 (79.0%)	0.58 (40.0%)

Figure 1 shows the cross-sectional view of the present configuration of the CDF detector. The central tracking system, immersed in a 1.5 Tesla cylindrical superconducting solenoid is surrounded by the calorimeters. The central calorimeter along the side of the solenoid is a scintillator-absorber sandwich calorimeter. The region $10^0 < \theta < 37^0$ ($1.1 < \eta < 2.4$) is covered by the end plug calorimeter and the region $2.4^0 < \theta < 10^0$ ($2.4 < \eta < 3.9$) is covered by a separate, forward calorimeter. These calorimeters, made of proportional tube-absorber sandwiches, were designed for the 6 × 6 bunch crossing condition. Due to an intrinsically slow signal from proportional tubes, an 800 nsec integration gate has been used.

The operational condition for Run II (36 × 36 bunches) will result in the reduction of the time interval between bunch crossings from the present 3.5 μsec to 396 nsec. In order to utilize the increase of the luminosity at the highest efficiency, possibly 80%

or better, the CDF has decided to replace the calorimeters in the end plug and the forward regions covering the angular region of $3.5^0 < \theta < 37^0$ ($1.1 < \eta < 3.5$) with a system with much faster response time.

1.2. Structure of the Upgraded End Plug Calorimeter

The experience of the CDF with the central calorimeter over the past ten year has proven the excellent long term stability of the plastic scintillator-based calorimeter. This fact, together with the very fast response time of the scintillator, prompted the CDF to select a plastic scintillator-absorber sandwich calorimeter for the upgraded end plug calorimeter.

In addition to the advantage of faster timing, the scintillator-absorber sandwich calorimeter will be much denser due to its higher sampling media compared to the gas proportional tube calorimeter. Using 23 layers of 4 mm scintillator and 4.5 mm lead plate clad with 0.5 mm stainless steel on both sides, the electromagnetic compartment (EM) will be 23 X_0 deep, compared with 18 X_0 depth of the present calorimeter. However it will take up only 60% of the physical depth occupied by the present system.

The increase in the density of the EM will also improve the hermeticity in the transition region between the central and end plug calorimeters. In the present configuration, the 37^0 region is one of the sources of the transverse energy and the missing transverse energy measurement degradation. Higher density of the EM calorimeter will also improve the hermeticity at the edges due to smaller Moliére radius reducing the electromagnetic shower leakage.

The existing steel structure, consisting of twenty one steel plates, each 5 cm thick, with 1.9 cm gaps in between acts as the return path of the solenoidal flux. It will be preserved in order not to alter the magnetic field map of the tracking volume. Layers of 6 mm thick scintillator inserted into the steel gaps will replace the present proportional tube layers in the hadronic compartment (HAD). The gap created by the shorter EM depth will be utilized by two additional HAD layers with stainless steel plates.

The present steel structure will be extended from $\theta = 10^0$ to 3.5^0 ($2.4 < \eta < 3.5$), as shown in Fig. 2a. The extension will eliminate the undesirable transition to a separate forward calorimeter. A significant side benefit of having a single calorimeter is that the forward muon toroid will be pushed up against the end plug wall. As a result the gap between the central muon detector, which presently extends up to $\theta = 40^0$ ($\eta = 1$) and the forward muon toroids, covering the region $\theta < 17^0$, will be almost eliminated. The future configuration of the upgraded CDF detector is shown in Fig. 2b.

The basic structure of the calorimeter will be a lamination of scintillator plates segmented into "tiles", interleaved with absorber plates, lead plates for the EM and steel plates for the HAD compartment. The EM and HAD will be segmented into the same projective towers. The transverse segmentation of the end plug calorimeter is shown on Fig. 3.

The new EM will be also instrumented with two layers of 5 mm wide scintillator strips placed at the fifth EM layer corresponding to $\approx 6\ X_0$ that will be used as a shower maximum detector (SMD). The strips will be oriented at an angle of $\theta = \pm 22.5^0$ with respect to the central line of each of $\Delta\phi = 45^0$ unit. The centroids of electromagnetic showers will be measured by the SMD to an accuracy of a few millimeters to check the matching with the incident charged track. Additionally, the measured shower profiles

will be used to examine the electron candidates and to reject π^0 contribution to the direct photon signal.

In addition, we are considering to use the first layer of the EM as a "pre-shower detector". The thickness of the materials in front of the calorimeter, the 5 cm thick aluminum end plate of the central tracking chamber and a 6 mm thick stainless steel plate, add up to 1.5 X_0, optimum for the discrimination of single γ from π^0 decays. The thickness of scintillator tiles would be increased to provide sufficient photostatistics. The pre-shower detector would have the same segmentation as the calorimeter towers.

The mechanical parameters of the upgraded EM, HAD and SMD are summarized in Table 3.

Table 3. Mechanical Parameters of the CDF Upgraded End Plug Calorimeter

EM	Absorber	4.5 mm Pb clad with 0.5 mm S.S. on both sides
	Scintillator	4 mm Polystyrene
	Total	23 layers
	Total thickness	35.7 cm (23.2 X_0, 0.96 λ_{int})
	Energy Sampling fraction	10.4%
	Density	0.65 X_0/cm
	Number of tiles	20448
	Number of Towers	960
HAD	Absorber	5.04 cm Fe
	Scintillator	6 mm Polystyrene
	Total	22 layers
	Total thickness	160 cm (6.8 λ_{int})
	Energy Sampling fraction	2.03%
	Number of tiles	16320
	Number of Towers	864
SMD	Scintillator	6 mm Polyvinyltoluene (PVT)
	Total	2 layers
	Number of Strips	6400

1.3. Tile-Fiber Readout

We have chosen to build the upgraded end plug EM and HAD as scintillator based sampling calorimeters employing the optical fiber readout technique. The schematic diagram of the fiber readout system of a calorimeter is shown in Fig. 4. The light from the finely segmented scintillator tiles is collected by the WLS-doped plastic optical fibers embedded in the tiles. Scintillator tiles are packaged with reflective wrapping, fibers and protective panels into "megatiles" as units of 15^0 for EM and 30^0 for HAD. Clear optical fibers spliced to the WLS fibers transport the light to the phototubes.

The optical cables are routed through the 2.5 cm gap between the central structure and the end plug to the rear of the calorimeter without sacrificing the hermeticity.

The SMD will also use WLS fibers for the readout. Each of the 5 mm wide scintillator strips will have a straight groove milled along the center line with a WLS fiber laid in the groove. Optical cables, common to the EM and HAD, will be used to guide the light to phototubes at the rear of the end plug structure. Multi-channel photomultiplier tubes (MCPMT'S) will be used to read out all the fibers individually.

1.4. Calibration procedures

The new calorimeter will have 1.3 mm diameter stainless steel tubes laid on the surface of the scintillator megatiles. The tubes (two per each 15^0 section) will pass through the lateral center of each tile. A Cs^{137} source encapsulated at the tip of a finer diameter tubing will be driven into these guide tubings enabling the calibration of all the tiles at their geometrical center.

The response of each tower will be calibrated when the end plug structure is in an extracted position. Such calibration should provide the correction for the overall light yield, including the effect of the transmission through cable-connector assemblies. In addition, the tubings for a limited number of layers, 5 for the EM and 4 for the HAD, will be brought to the rear of the detector for the in-situ calibration.

2. Tile-Fiber R&D Results

Following the construction and beam tests of prototype modules for EM and HAD[1] we have undertaken an extensive R&D program.[2] The goal of this effort was to optimize the design of the optical readout system and to make the production techniques viable for the full-scale detector. Significant improvements have been achieved over the techniques employed in the construction of the prototype modules. An extensive study has been carried out for the selection of the materials and optimization of the tile/fiber configuration.

First, we chose the σ pattern[3,4] of the WLS fiber layout in a tile. Figure 5a shows the pattern of the fiber layout in a tile. In this case only one end of a complete loop of the WLS fiber is spliced to a clear fiber, while the other end is mirrored.[5]

Secondly, we developed fiber connectors and optical fiber cables which allow to separate mechanically the optical system into three sections. The first section brings the light produced by the tiles to the edges of the megatiles where optical connectors are placed, as shown on Fig 5b. The second section consists of optical fiber cables that bring the light to the backplane of the plug. The last section is a decoder-box which rearranges layer-to-layer arrays of fibers in the optical cables into tower-by-tower bundles that will be connected to phototubes.

The reduction of the number of readout fibers and the introduction of the optical connectors lower the absolute light yield of tile/fiber assemblies. However, a newly developed multiclad fiber[6] allowed us to compensate for this reduction of the light output. The multiclad fibers have a polystyrene core with the index of refraction, n=1.59, and PMMA (n=1.49) and a fluorinated polymer (n=1.42) as the inner and the outer cladding *. The use of a cladding material with lower index of refraction

*The cladding in single clad fibers is PMMA, (n=1.49).

increases the trapping efficiency of light to 5.35%, compared to 3.14% for a single clad fibers. Higher trapping efficiency of multiclad fibers increases light yield of the tile/fiber assemblies by 50% to 70%.

In the following sections we describe the energy resolution and uniformity requirements of the upgraded end plug calorimeter. We then present some of the R&D results leading to the final design of EM and HAD plug calorimeters.

2.1. Energy Resolution and Uniformity Requirements

Based on the beam test results of the prototype module and the results from R&D, the expected energy resolutions are $\sigma/E = 17\%/\sqrt{E} \oplus 1\%$ for the EM compartment and $\sigma/E = 80 - 90\%/\sqrt{E} \oplus 5\%$. In order to achieve such energy resolution for the EM the overall response of the scintillator tiles has to be uniform to a level of r.m.s of 10% within each tower and of r.m.s. of 2% over the surface of each tile.

The requirement for the HAD is looser, since its design is constrained by the mandate of preserving the existing steel structure of 5 cm thick steel plates. The design energy resolution can be met, if the tile response is maintained to 20% r.m.s. for tile-to-tile variations.

2.2. Uniformity of Response of Tile/Fiber Assemblies

We have studied techniques to produce tiles with uniform response over their entire surface. In the past[1-7] we have used the correction masks to improve the uniformity of the light collection of tile/fiber assemblies. Recently a simpler method, based on a adjustment of the depth of the fiber groove has been developed.

Figure 6 shows the uniformity of the response of the tiles with different depths of the grooves. We used 4 mm thick, 10.8 cm $\times$ 10.8 cm SCSN-38 tiles, with the σ fiber layout pattern. The edges of the tile were painted with white reflective paint and wrapped with aluminized mylar. A green WLS fiber Bicron[8] BCF-91A, 0.83 mm in diameter, spliced to 3 m of clear Kuraray fiber was inserted into the tile. The width of the fiber groove was 0.95 mm. Tiles with three different depths of fiber groove: 1 mm, 1.6 mm and 2.5 mm were investigated.

The results indicate that the optimal uniformity of the response of 4 mm tiles of this size is achieved by choosing the groove depth of 1.6 mm. The r.m.s. of the uniformity of response is approximately 2%. For the EM tiles, the depth of the fiber grooves is further optimized as a function of the tile size. A similar study indicated that the optimal transverse uniformity of 6 mm thick scintillator tiles can is achieved for the fiber groove depth of approximately 2.5 mm.

2.3. Light Yield of Tiles as a Function of their Size

In the projective geometry, the tile sizes vary significantly as a function of an angle and a depth of the layers. In order to achieve the specified uniformity of response of the tiles, it is important to understand the variation in the light yield of the tile/fiber assemblies as a function of the size of the tiles.

We have measured the light yield of tiles with transverse sizes ranging from 10.8 cm $\times$ 10.8 cm to approximately 30 cm $\times$ 30 cm. The measurements were done using a 0.75 mm in diameter, 90 cm long WLS green fiber BCF-91A, spliced to 3 m long single clad clear Kuraray fiber.

Figure 7 shows the relative light yield of the tiles, as a function of the parameter l/A, where l is the length of the green fiber imbedded inside the tile and A is the area of the tile.The plot indicates that the relative light yield of the tiles scales approximately with the parameter l/A. The scaling of the light yield with the parameter l/A indicates that the average response of the tiles within a tower can be uniformized by varying the length of the WLS fiber groove inside the tiles. This adjustment can be achieved, for example by changing the distance between the location of the fiber groove and the edge of the tile.

2.4. The EM and Hadron Calorimeter Material Choice

Table 4 summarizes the technical data of scintillator and fibers used in the assembly of the EM and Hadron megatiles. The SCSN-38 scintillator is a blue polystyrene

Table 4. Summary of the materials used in construction of EM and HAD calorimeters. Scintillator and fibers used in the production of the EM and HAD are produced by the Kuraray.

application	material type
scintillator (EM)	4 mm thick, SCSN-38
scintillator (HAD)	6 mm thick, SCSN-38
WLS fiber	Y11 (250ppm), 0.83 mm dia., multiclad
clear fibers inside megatile	0.83 mm dia., multiclad
clear fibers for cables	0.90 mm dia., multiclad
clear fibers for decoder box	1.00 mm dia., multiclad

based scintillator with emission peak at 490 nm. It has been used for the central electromagnetic calorimeter. The green wavelength-shifting fiber uses Y-11 shifter, peaking at 510 nm. Blue scintillator is generally very fast and the pulse shape is mostly determined by the waveshifter. The wave shifters in the green spectrum are on the order of 10 nsec in the exponential fall time constant. Integration over 40 nsec will yield 98% of the signal well suited for the time constraint even for the possible future operation of the Tevatron with 132 nsec bunch crossing time.

3. Fabrication Techniques and Optical Elements

3.1. Fiber Polishing Technique

As shown in Table 3, the total number of fibers used in this project will be approximately 80,000. As a consequence, a proper technique is required to handle such a large number of fibers. The very basic process is to cut the fiber ends properly. The ends of the fibers should be smooth, flat, perpendicular to the fiber axis and without chipping of the core or the cladding.

Many methods have been explored from cutting with razor blade to molecular bond scission by excimer laser. Finally we found that diamond flycutting, which is a commonly used technique for cutting plastic material, was applicable to a single fiber cutting. Two types of machines using the flycutting technique have been designed and

constructed. One of them is a portable machine of $\approx$ 12 kg, the other is designed for the mass production.

Two diamond bits are mounted on the flat surface of a wheel of 1.6 cm in diameter which rotates at a speed of $\approx$ 15,000 RPM. The diamond bits are mounted at the slightly different heights from the surface and the different radii on the wheel. When the wheel sweeps across the surface of the fiber, one of the diamond cuts the fiber first and the second diamond removes the material off the fiber with a predetermined depth. After removing about 0.5 mm in the fiber depth, the finish is very consistent.

Though the polystyrene core is always cut cleanly we encountered a problem of the chipping off the cladding at the point where the diamond exits perpendicularly to the unsupported cladding layer. The chuck extends up to a small distance from the plane of the diamonds. The solution for this problem was to use a sacrificial plastic sheath to support the fiber. The sheath is cut together with the fiber so that the cladding is supported to the end of the cutting cycle. The sheath does not need to have a tight fit to the fiber.

Since the diamond bit has a round edge, it leaves a wave on the fiber surface. The wave characteristics depend on the radius of the diamond, the speed of rotation of the wheel and the speed at which the fiber surface is swept.The machine was designed so that all these parameters can be adjusted within a certain range. However if one takes a set of parameters comfortably inside the adjustable range one finds that the residual wave is negligible for practical purposes for our application. Using the above described technique of fiber polishing allows us to mirror fiber ends with the reflectivity of 85%.

So far ten portable units have been built. All of the fibers ranging from 0.83 mm to 1 mm in diameter presently used at Fermilab from the CDF, D0 and KTeV experiments have been processed by either of the two types of machines. The diamonds remain sharp even after a significant amount of fibers have been processed.

3.2. Fiber splicing technique

As described before, each WLS fiber from the scintillator tile has to be spliced to a clear fiber. Methods of splicing two fibers thermally fusing their joint have been developed by the CDF[9] and have been further refined.[10] Two types of machines have been developed for mass production. In either case, two fibers to be spliced are pushed together in a plastic sleeve, laid in a pair of tight-fit half-shells of a quartz tube and the junction is heated.

The method used for the construction of the HAD megatiles uses an halogen lamp with a focusing reflector. A FEP sleeve is pre-fit to the fibers and a region of approximately 5 mm around the junction is melted. The bonding was measured to withstand up to 4 kg in tension. The tests have indicated that this method works only for non-S type fiber from Kuraray.

The other method is being applied for the EM production and uses a sleeve made of PEEK heated by a single Nichrome wire laid underneath the junction. The fiber is melted in a narrow region around the junction. Since the bonding strength is only 1.5 Kg, glue is smeared over the fibers at both ends of the sleeve prior to the heating. This method works for S-type fibers from Kuraray.

An extensive study was carried out to find the range of optimum performance. Though there is a reasonable range of conditions in each of the control parameters, it

was found that the location of the heating wire and the fitting of the sleeve are rather critical factors to be tuned.

After rejecting faulty splices by a visual inspection, both methods yield approximately 91-92% of light transmission across the splice, with an r.m.s. variation of 2%. A test showed that if the two ends are simply cut with a razor blade, the results tend to scatter more than when the fibers end are prepared with the diamond cutting machine.

3.3. Optical Fiber Cable

Similarly to the situation of ordinary electrical wires, a large number of optical fibers has to be grouped properly both for mechanical protection and to to prevent confusion in the fiber connections. We have developed optical plastic fiber cable with ten 0.9 mm fibers assembled into a flat ribbon cable. The fiber spacing is 1.4 mm and the fibers are protected with 50 μm thick jacket made of black Tedlar.[11] Since the jacket is thin, there is enough flexibility determined by the fibers themselves. We have tested the loss in the light transmission in the cable as a function of its radius of curvature. The study included also an aging test performed using the heat cycles. The result, similar to what has been observed with single fibers, showed no deterioration for the fiber bending radii of 1.5 cm or larger.

3.4. Fiber Connectors

It is natural to terminate an optical fiber cable with connectors at both ends. The fibers from the tiles are also terminated by connectors mounted on the edge of the megatile. The connector provides the capability of connecting/disconnecting between the megatile and the phototube. Figure 8 shows the design of the HAD connector.

The most important feature of a connector is more in its reproducibility than in its absolute light transmission. Therefore, it was decided to leave the junction with air gap without optical grease. Figure 9a shows the light transmission across the connector. The total light loss is on average 17%, 10% of which is accounted for by inevitable Frenel reflection.

The reproducibility of the light transmission after multiple dis- and re-connecting is plotted in Fig. 9b. It should be noted that the variation of absolute light transmission of individual light path from a scintillator tile to a phototube is added in quadrature to the intrinsic tile response variation in a tower which is required to be better than 10% (in case of the EM). Therefore the measured distribution of the reproducibility of about 1-2% satisfies the requirement. The variations of the light transmission of each light path in the cable-connector assembly also affect the tower-to-tower uniformity, which is required to be 2%, collectively.

4. Megatile Production procedure

The design of the calorimeter requires a large number of towers implying even larger number of tiles. In order to limit the number of individual elements in each sampling layer, the tiles of each 30 degree section of the calorimeter are grouped into a single mechanical unit called megatile.

All 32 tiles within a 30^0 section of the HAD are cut from a single piece of a scintillator sheet. Separation grooves between the tiles are milled out by a computer controlled machine, leaving $\approx$ 0.25 mm of uncut scintillator at the bottom of the groove.

The grooves are then filled with a white paint/epoxy mixture[12] to glue the individual tiles together. The epoxy is used for both the structural support and as a reflective surface at the edges of the tiles. A black marker is used to paint a line on the surface of the scintillator between the tiles to minimize the light cross talk. As shown in Fig. 10, the light cross-talk between neighbouring tiles is less than 2% per edge of the tile.

After the glueing procedure is completed, the megatile is put back on the milling machine and the fiber grooves are cut out. In the next step, the scintillator sheet is wrapped using white reflective material, Tyvek.[13] Then, a layer of plastic with grooves to route clear fibers is placed on top of the scintillator sheet (see Fig. 11). At the final assembly stage, the fibers are inserted into all tiles and the megatile is covered with black Tedlar[11] for the light-tightness purpose and placed in the aluminium pans for the mechanical protection.

Production and assembly of the EM follows a similar pattern. EM tiles are however individually cut, arranged into 15^0 units and mechanically fixed onto protective plastic panels using plastic scintillator pins.

4.1. Quality Control of Tile/Fiber production

The quality control program of the calorimeter production is designed to monitor the light yield variations of individual tiles. Below we describe the quality control procedures for the HAD production. A similar set of procedures is being applied in the EM production.

The thickness of each scintillator sheet was measured at several points by the manufacturer. The variation in thickness of scintillator sheet does not exceed 2% r.m.s. In addition, the manufacturer has tested samples of scintillator for the absolute light yield and the attenuation length.

The quality of incoming fibers is monitored by testing relative light yield and attenuation length of sample of the WLS fibers as well as the attenuation length of clear fibers. The r.m.s. variation of the relative light yield of WLS fiber was $\approx 4\%$, and the variation of attenuation length of the WLS and clear the fibers was $\approx 2\%$ and 3% respectively.

After the WLS fibers are mirrored, spliced to clear fibers and glued into connectors, each fiber/connector assembly is tested for the relative light yield and the transmission across the splice using a setup employing UV lamp and photodiode readout. Figure 12a shows the distribution of the relative light yield of fibers before the insertion to a megatile. The typical r.m.s. of this distribution is approximately 3-4%. Fiber/connector assemblies containing the fibers with relative light yield outside of $\pm$ 10% cut are rejected. After the insertion of the fibers into tiles, the fully assembled megatiles undergo the final quality control test. The relative light yield of each individual tile in the megatile is recorded using using a computerized Cs^{137} γ source scanner. Figure 12b shows the distribution of the relative light yield of tiles from a set of four megatiles. The r.m.s. of the distribution is less than 6%, well within the requirements for the tile-to-tile variation.

5. Shower Maximum Detector

5.1. Introduction

The SMD is a position sensitive detector placed at a depth of approximately 6 X_0 inside the EM calorimeter. Its purpose is to measure centroids and the lateral profiles of the showers to help the separation e's and γ from π^0.

The active detector elements are scintillator strips read out with WLS fibers. The feasibility of this design has been amply proven in the past.[14,15] The WLS fibers are connected through optical connectors to clear fibers that carry the light to MCPMT's located at the rear of the end plug structure.

5.2. Design Criteria

The SMD will cover a circular area of 2.6 m in diameter at both ends of the CDF detector at 1.8 m from the nominal interaction point at B0 . It will be made of two identical sectors covering 45^0 in ϕ, each sector consisting of two layers of scintillator strips arranged in directions parallel to the sector's sides (Fig. 13). The strip directions in these layers will be referred to as U and V.

The design of the detector is constrained by the overall design of the plug calorimeter. The 45^0 ϕ segmentation was chosen as a multiple of the calorimeter segmentation. Monte Carlo studies show that the π^0 rejection efficiency increases with U-V crossing angle, and angles greater than 15^0 are necessary for good efficiency. Crossing angles greater than 45^0 are not feasible mechanically.

Both the U and V sectors are divided into segments covering the pseudorapidity regions $1.1 < \eta < 2.6$ ($8.5^0 < \theta < 37^0$) and $2.6 < \eta < 3.5$ ($3.5^0 < \theta < 8.5^0$). Every sector will house 400 strips, 5 mm wide and 6 mm thick, for a total of 6,400 channels. The sectors will fit in the 21 mm slot reserved in the fifth layer of the EM calorimeter.

Test beam studies and simulations show that a channel-to-channel calibration of 10% or better is necessary for a good position resolution and π^0/γ discrimination power. Since presently available MCPMT's have generally larger gain variations between channels, we consider careful channel by channel calibration of this detector as crucial factor. Because of scintillator aging and potential radiation damage, it is necessary to monitor the calibration during the course of the run. The calibration scheme discussed in section 5.6 satisfies these requirements.

5.3. SMD Performance Simulation

A detailed detector simulation study has been performed to investigate the effect of varying design parameters such as strip width, depth and relative angle. In addition photostatistics, gain, crosstalk, and dead space between the SMD strips have been studied.

Electrons, photons, and π^0's were generated using the GEANT 3.14 package and the SMD was simulated at various depths within the calorimeter using a 45^0 crossing angle between the U and V layers of 6 mm thick scintillator strips at a 5 mm pitch.

Figure 14 shows the π^0 rejection for both 80% and 90% γ-acceptance versus incident particle energy. For the 80% γ-acceptance the π^0 rejection varies from 90% for 10 GeV π^0's to 50% for 90 GeV π^0's. Also shown is the position resolution versus incident particle energy for e and γ's. The resolution is 1.5 mm for 10 GeV electrons

and better than 1 mm for energies greater than 30 GeV. Both the π^0 rejection and position resolution are optimal, for 47 GeV particles, at a depth of five EM calorimeter layers (5.5 radiation lengths). The showers are not sufficiently developed at smaller depths and spread out too much at larger depths.

The SMD performance improves with an increasing crossing angle. The π^0 rejection does not improve dramatically, but the position resolution in the θ dimension is very sensitive to the crossing angle.

The SMD position resolution and π^0 rejection improve when the SMD is placed in front of the EM calorimeter tile sharing the same slot due to the very soft component from the lead layer.

The effect of light yield on the SMD performance was studied by digitizing the energy deposited in the SMD strips in terms of photo-electrons. The π^0 rejection and electron position resolution degrade at low energies for light yields less than 1 photo-electron per MIP. We set 2 photo-electrons per MIP as our minimum requirement in light yield for the choice of the scintillator-WLS fiber combination.

In order to estimate how well we need to cross calibrate the SMD strips, channel to channel gain fluctuations were simulated. Gain fluctuations of up to 10% did not significantly affect either the π^0 rejection or the position resolution.

Because all the MCPMT's tested so far have crosstalk to adjacent channels, the effect of crosstalk on SMD performance was simulated. The effect of 20% crosstalk on position resolution was not apparent. However the effect of 10% crosstalk on the π^0 rejection could be seen for energies above 60 GeV.

All construction techniques require a finite amount of dead space between the SMD strips. Dead space between the SMD strips had a noticeable effect on the position resolution but only slightly decreased the π^0 rejection. The position resolution for 47 GeV γ's went from 0.67 mm with no dead space, to 0.71 mm with 0.25 mm dead space, and 0.76 mm for 0.75 mm dead space.

5.4. Panel segmentation

The scintillator-strip layers are segmented into two parts, the high-η region ($2.6 < \eta < 3.5$) and the and low-η region ($1.1 < \eta < 2.6$). The main reason for η–segmentation is to reduce the occupancy of the strips expected from the underlying minimum bias event. The occupancy of a single strip in a minimum bias event can be calculated analytically.

In the limit of small angles,

$$\eta = -\ln\tan(\theta/2) = -\ln(r/2L)$$

where r is the radius on the SMD plane and L the distance from B0, which is taken to be 184 cm. For a flat particle distribution as a function of η, which is approximately the case up to the largest value of $\eta = 3.6$, we have

$$dN/drd\phi = -c/2\pi r$$

where c = 4.8 γ 's, the average number per unit η expected from minimum bias π^0's. For strip width a, $d\phi = a/r$, so that

$$(dN/dr)_{strip} = -ca/2\pi r^2$$

Table 5. Scintillator Strip Occupancy for the SMD

$r_1(cm)$	η_1	$\pi_1^0 - GeV$	$r_2(cm)$	η_2	$\pi_2^0 - GeV$	N_{strip}	N_{ave}
10	3.6	9.2	133	1.1	0.9	0.035	0.018
10	3.6	9.2	28	2.6	3.3	0.024	0.040
28	2.6	3.3	133	1.1	0.9	0.011	0.011

If the strip runs from radius r_1 to r_2, the occupancy is

$$N_{strip} = (ca/2\pi)(1/r_1 - 1/r_2)$$

In our case, c = 4.8 and a = 0.5 cm, so that $ca/2\pi = 0.38cm$. For r_1 = 10 cm and r_2 = 133 cm the occupancy of the strip is 3.5% (for a single event). Table 5 lists some other interesting values and parameters:

Although the occupancy expected in the high η–segment is approximately two to four times larger than that of the low η segment, further segmentation was found to be impractical.

5.5. Light Yield Studies

THe SMD detector is located at the shower maximum position where the radiation is relatively high and the ratio of active volume to surface area is much lower for the strips than for normal tiles. To avoid any potential problems caused by chemicals we decided to wrap the SMD strips in 25 μm thick aluminum foils without any glue or paint.

Tests of the response of the detector were studied at the far end of the longest strip which corresponds to the lowest light yield region. The measurements were done with 100 cm long WLS fiber going directly to a PMT (Philips XP2081). This configuration measures the amount of light reaching the connector at the edge of the SMD layer. There is an additional reduction factor of 0.5 in the attenuation coming from the optical connectors and the clear fiber assembly used to bring the light to the rear of the end plug. We also have to take into account an additional reduction factor of 0.3 corresponding to the ratio between the QE of the PMT used in the measurements and the the effective quantum efficiency of a MCPMT due to the "excess noise factor". The list of materials tested in a wide range of combinations is given in Table 6.

The measurements were performed using a scanning electron gun with a 3 MeV electron beam from a Ru^{107} . The spectral response of the test strips was recorded the absolute light yield was computed, as shown in Fig. 15. The setup was calibrated with a set of reference tiles before each measurement.

For the purpose of the light yield comparison, the results of 4 mm scintillator samples was extrapolated to the 6 mm thickness. The final results of the most promising combinations are given in Table 7. The light yield values correspond to the averages over 14 measurements and the errors are equal to the r.m.s. of the measurements. In this study we used the highest light yield fibers, i.e. Y11 - 350 ppm multi clad, 0.83 mm fiber with a polished and mirrored end. Taking the reduction factor of 1/6 to

Table 6. Materials Tested in the SMD Light Yield Studies

scintillator (company)	WLS fiber (company)
BC404 (Bicron)	BCF91A (Bicron)
BC408 (Bicron)	BCF92 (Bicron)
BC404A (Bicron)	Y11-75 ppm St. Cl. Non S-Type (Kuraray)
SCSN38 (Kuraray)	Y11-150 ppm St. Cl. Non S-Type and S-Type (Kuraray)
SCSN62 (Kuraray)	Y11-250 ppm St. and Ml. Cl. S-Type (Kuraray)
	Y11-350 ppm St. and Ml. Cl. S-Type (Kuraray)

estimate the number of photoelectrons in the MCPMT, the only scintillators surviving the minimum requirement of 2 photo-electrons per MIP, are Bicron BC404, BC404a and BC408.

Table 7. Highest Light Yielding Combinations

scintillator	fiber	Photoelectrons/MIP
BC404	Y11-350 ppm Ml.Cl. al. 1 m S-type	14.20 ± 0.18
BC404A	Y11-350 ppm Ml.Cl. al. 1 m S-type	12.99 ± 0.36
BC408	Y11-350 ppm Ml.Cl. al. 1 m S-type	12.98 ± 0.39
SCSN38	Y11-350 ppm Ml.Cl. al. 1 m S-type	10.08 ± 0.25
SCSN62(4 mm)	Y11-350 ppm Ml.Cl. al. 1 m S-type	8.10 ± 0.30

5.6. Calibration Scheme

A mechanism identical to the calorimeter tile calibration scheme will be used to monitor the chain of SMD strips and MCPMT's. A Cs^{137} source encapsulated in the tip of a fine wire will be driven through a guiding tube running almost perpendicular to the strips in the SMD plane. The current read-out on the MCPMT will provide the relative calibration between the strips.

Figure 16 shows a simple setup used for preliminary studies of the wire source calibration. Five individual strips were assembled together and were read out by 5 individual PMTs. A source wire was run in a tube crossing the strips as shown in Fig. 16. Also shown is the DC current response of the strip, as a function of the position of the source wire inside the tube during the insertion (first 2 peaks) and the extraction (last 2 peaks) of the source wire.

The reproducibility of the peak height was about 1%. In order to test the "wire sourcing+peak finding" algorithm, we manually changed the gains of the calibrated PMTs. We were able to determine the change in gains at a level of 5% using the source data. Further studies are in progress to determine other systematic effects such as the positioning of the source tubes with respect to the scintillator strips.

5.7. Mechanical Assembly

The SMD fiber grooves and strips are cut at Fermilab using a computer controlled milling machine. The SMD strips are then machine-wrapped with aluminized mylar using the Fermilab magnet winding machines. Groups of 10 wrapped SMD strips are taped together to form a megastrip.

A test indicated that the light yield decreases as the strips become shorter. For efficient light collection, the strip length should not be smaller than 5 cm (Fig. 17). For this reason, and also for the reason of avoiding very short strips, the short–strip–corner of the high-η sector is serviced by strips from the low-η sector. The short strips of the low-η sector are eliminated as shown schematically on Fig. 18.

The cover plates are cut out of polycarbonate sheets and grooved using the milling machine. Megastrip separators are inserted (Fig. 19) and the megastrips are placed and taped down using these separators. Three megastrips will service the high-η sector. Their WLS-fibers will be spliced to clear fibers that are routed underneath the scintillator strips of the low-η sector in the grooves cut in the polycarbonate covers.

The WLS fibers are cut, polished, mirrored and spliced (for the high-η sector only). The fibers are then inserted into the optical connectors, cut to length, glued and polished. The final fiber/connector assemblies are tested for uniformity and the light transmission. Fully assembled, identical U and V pans are screwed together with the polycarbonate covers on the outside, resulting in the 45^0 relative angle between the planes. Quality control tests are performed at this point to assure a positive feedback on the construction technique using cosmics, collimated sources, and wire sources driven through the tubes in the polycarbonate cover.

Acknowledgements

We wish to thank many technical staff members of the Fermilab Physics Department and the Technical Support Services whose help was essential in the undertaking of this project. This work was in part supported by the U.S. Department of Energy, Grant No. DE-FG02-91ER40685 (U. of Rochester), DE-FG02-91ER40651 (Rockefeller U.) and Contract No. DE-AC02-76CHO3000 (Fermilab).

References

1. M. Lindgren at al., published in the proceedings of the Third International Conference on Calorimetry in High Energy Physics, Corpus Christi, TX, 1992, ed. by P. Hale and J. Siegrist, World Scientific, 1993.
2. P. de Barbaro et al., University of Rochester preprint UR1299, 1993, SDC-93-407.
3. P. de Barbaro et al., Nucl. Instr. and Meth. A315 (1992) 317.
4. G.Apollinari, CDF Note 1847 (1992).
5. The mirroring of fiber ends in done at Fermilab facility using magnetron gun sputtering technique. The thickness of aluminum deposit on WLS fibers is ≈ 1500 $\AA$.
6. Kuraray International, 200 Park Ave., New York, NY 10166.
7. Proposal For an Upgraded CDF Detector, Oct. 1990, CDF Note 1172.
8. Bicron Inc., 12345 Kinsman Rd., Newbury OH 44065-9677. White reflective paint, BC-620 from Bicron Inc.
9. G. Apollinari, D. Scepanovic and S. White, Nucl. Instr. and Meth. A311 (1992) 520.
10. Detailed description of the splicing device build by the Michigan State University group can be found in C. Bromberg et al., New Methods in Optical Fiber Preparation for Scintillating Tile Calorimetry in CDF, to be published in the proceedings of the IV International Conference on the Calorimetry in the High Energy Physics, La Biodola, Elba, Sept. 1993.
11. Tedlar is trademark of a thin, black material produced by the Du Pont Co.
12. The white paint/epoxy mixture was prepared by milling TiO_2 with the epoxy resin (DER332 by Dow Chemicals) in 1:2 weight ratio. Then white paint/epoxy mixture was combined with the hardener (Jeffamine (TM) Polyoxypropyleneamines D-230 by Texaco): for 100 g of white paint/epoxy mixture we add 21.3 g of D-230 hardener.
13. Tyvek is trademark of a white reflective material produced by the Du Pont Co. E.I. Du Pont de Nemours & Co., Fibers Department, Chestnut Run Plaza, PO Box 80,705, Wilmington, DE 19880-0705. The HAD megatiles are wrapped with 1055B 'Housewrap' Tyvek.
14. G. Apollinari, IEEE Trans. Nucl. Sci. Vol. 40, N.4 (1993) 484, K. Goulianos et al., NIM A324 (1993) 475.
15. M. Hulbert et al., SDC-92-343 (1990).

Figures

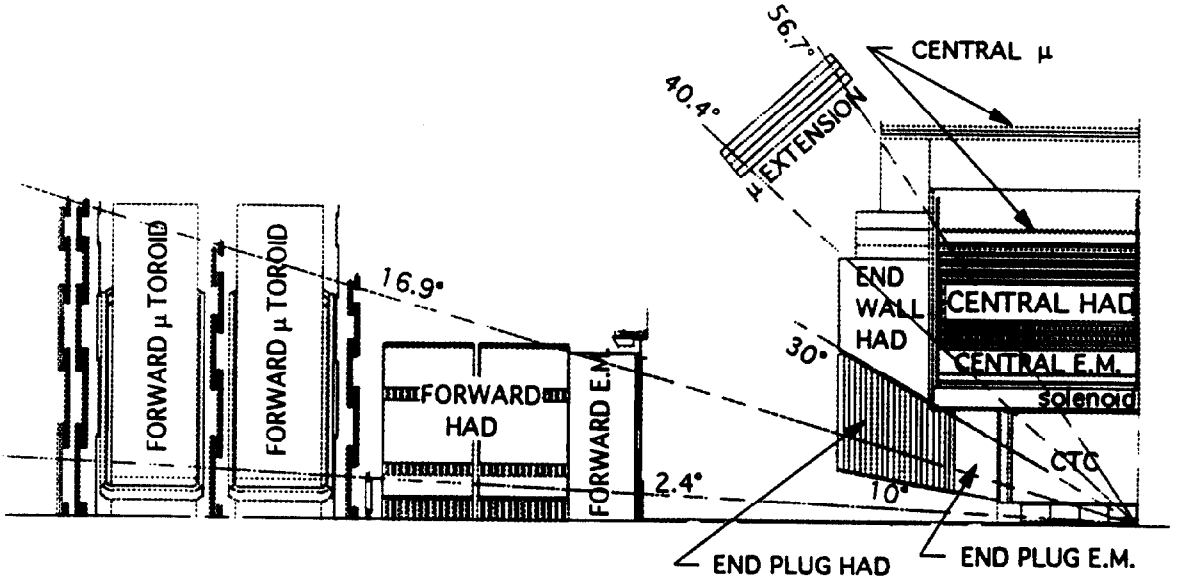

Fig.1: The cross sectional view of the present configuration of the CDF detector.

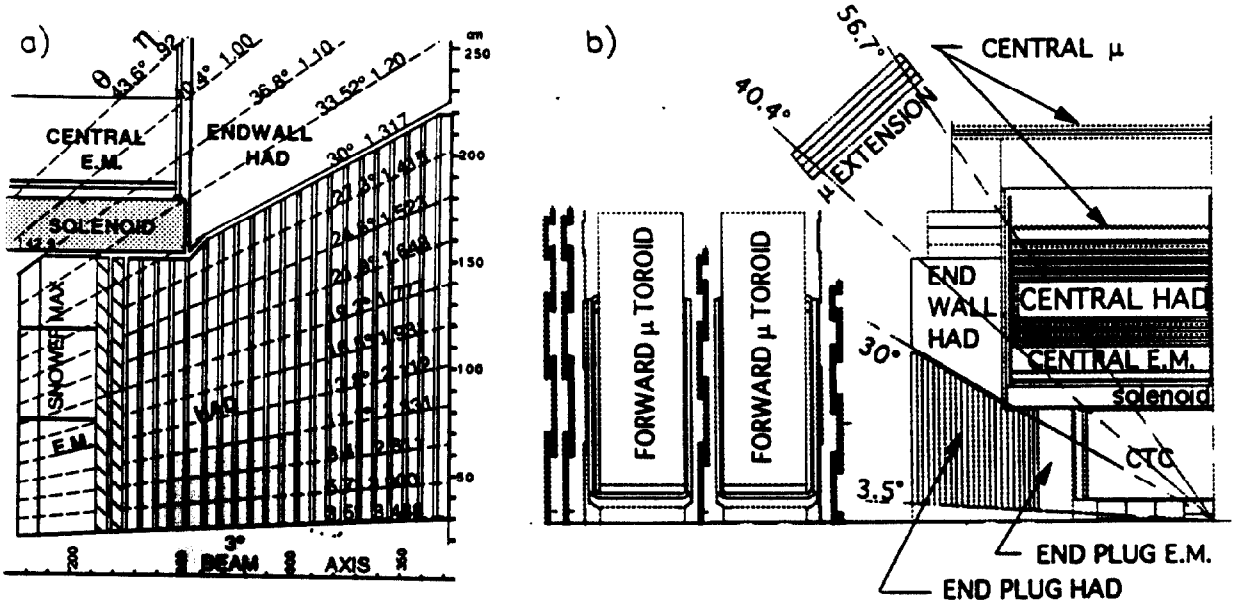

Fig.2: a) The structure of the upgraded End Plug Calorimeter.
b) Cross sectional view of the upgraded CDF detector.

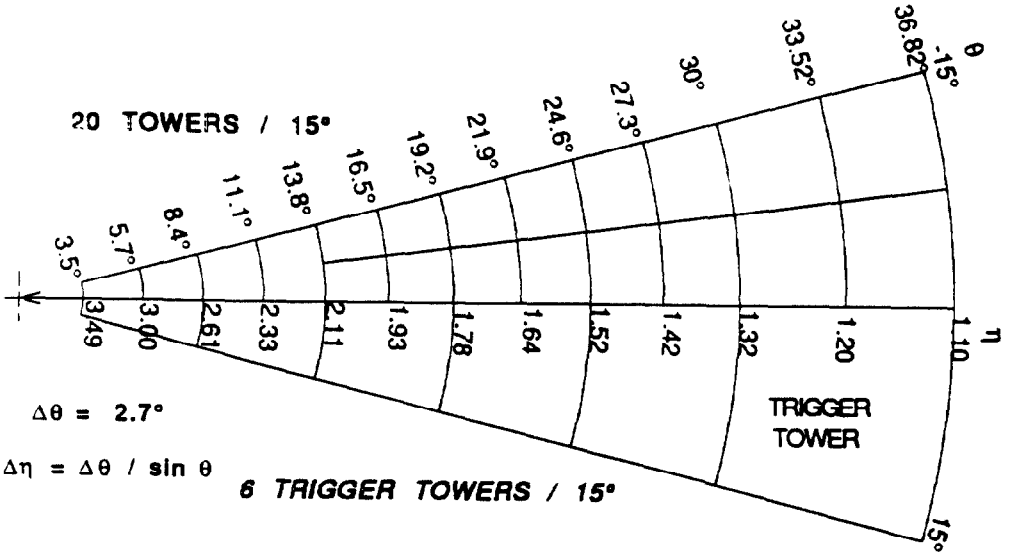

Fig.3: The transverse segmentation of the upgraded End Plug Calorimeter.

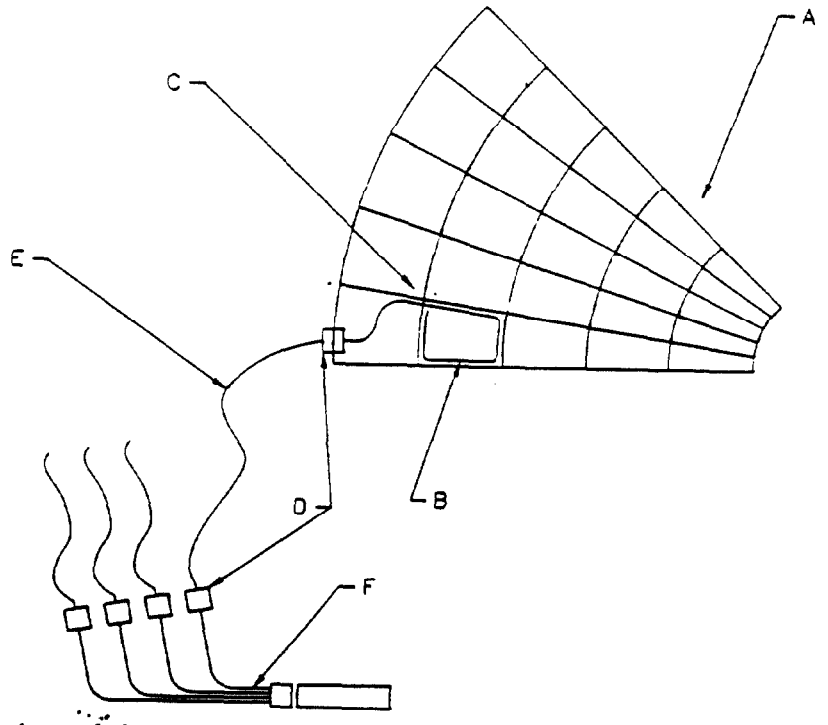

Fig.4: Generic view of the optical fiber readout system of a calorimeter: a) scintillator sheet segmented into optically isolated and mechanically bond tiles; b) green WLS fiber with one of the ends mirrored; c) green-to-clear fiber splice; d) optical fiber connectors; e) optical fiber cables carrying the light to the back of the calorimeter; f) decoder box rearranging fibers from layer-to-layer cables to tower-to-tower bundles.

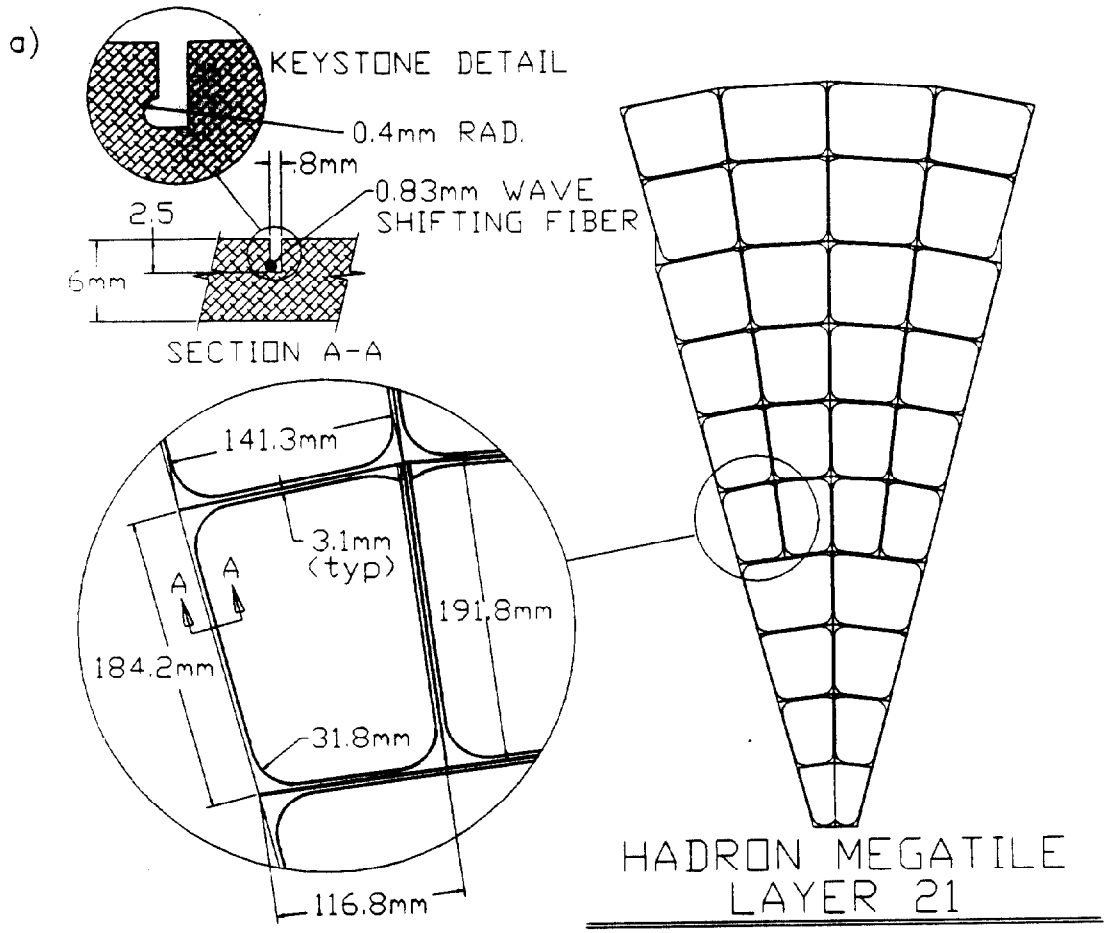

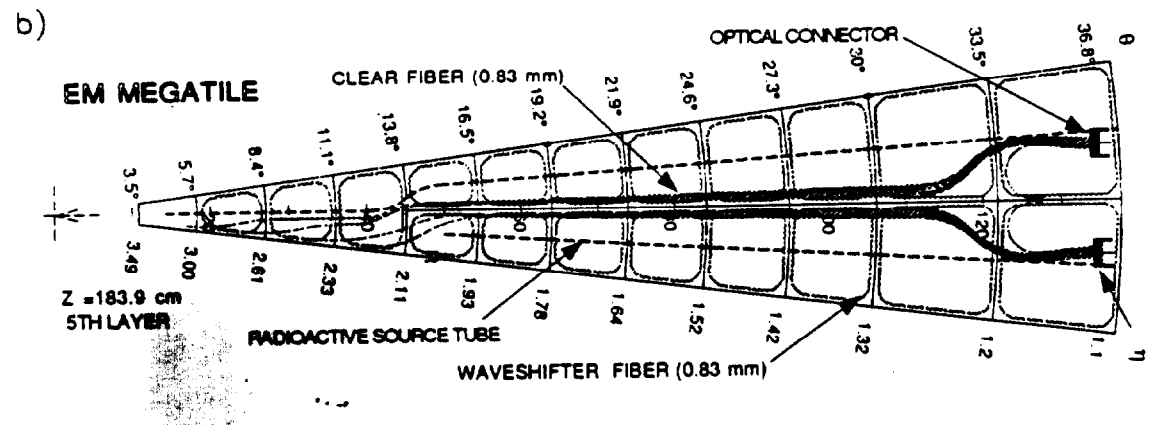

Fig.5: a) The pattern of the WLS fiber layout for a HAD megatile (layer 21). The distance between a tile edge and a fiber groove is approximately 3 mm, the radius of fiber bend is $\approx$ 3 cm. The figure also shows the cross-section of a fiber groove. The dimensions on the drawing are expressed in millimeters.
b) The pattern of the WLS and clear fiber routing for a 15^0 EM sector (layer 5).

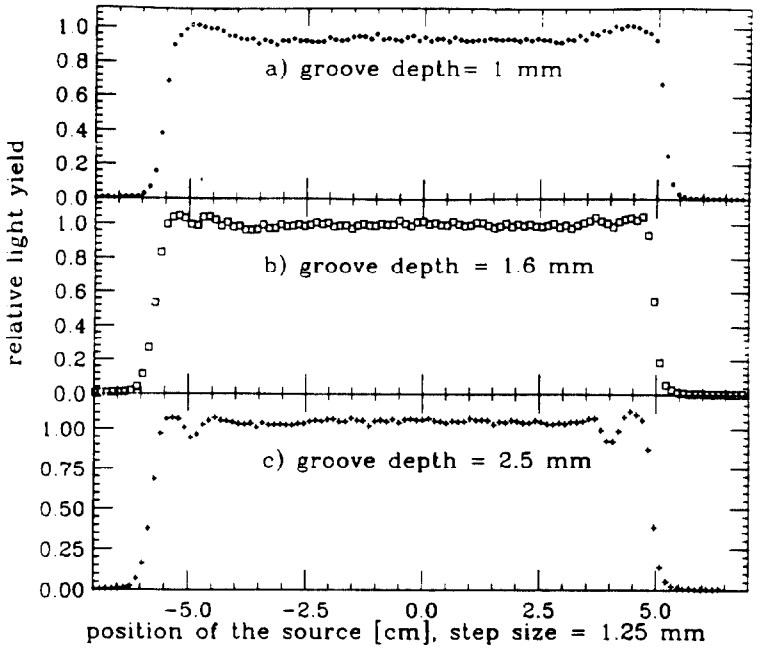

Fig.6: Transverse scan of 4 mm thick tile with different depth of fiber groove: a) 1 mm deep; b) 1.6 mm deep; c) 2.5 mm deep. The light yield of the tile relative to the average light yield of the tile with 1.6 mm deep groove is plotted as a function of the position of the electron source. The width of the groove is equal to 0.95 mm. The transverse dimensions of the tile were 10.8 cm × 10.8 cm. The diameter of WLS fiber used was 0.83 mm.

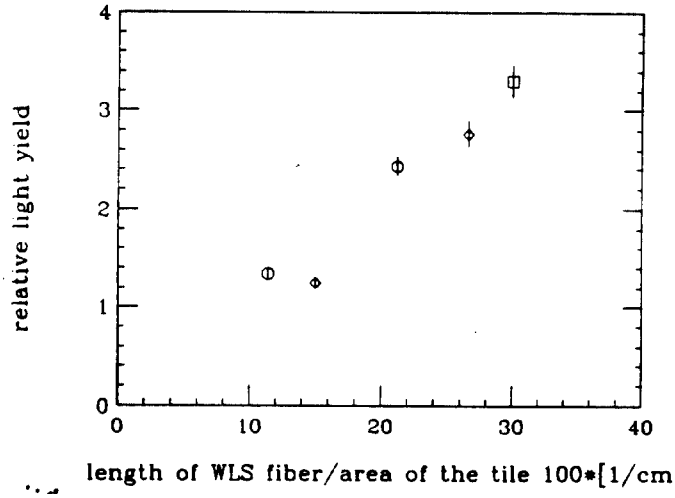

Fig.7: Light yield of various tiles plotted as a function of a parameter l/A, where l is the length of the WLS fiber inside the tile, and A is the area of the tile. Tiles from different projective towers are represented by the different symbols. From geometric considerations one expects that the average light yield of a tile would scale with the variable l/A.

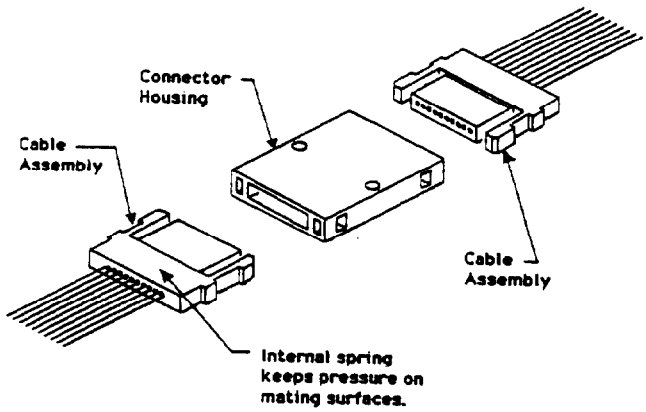

Fig.8: The schematic drawing of the HAD connector.

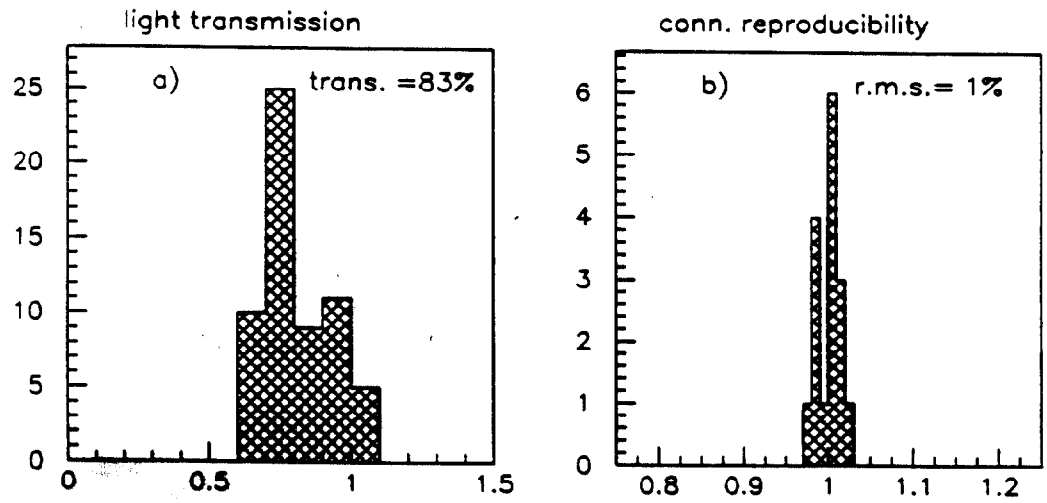

Fig.9: a) Distribution of the light transmission across a fiber connector. The average transmission is 83%.
b) Reproducibility of the light transmission of a fiber connector for multiple dis- and re-connecting. The r.m.s. of this distribution is less than 2%.

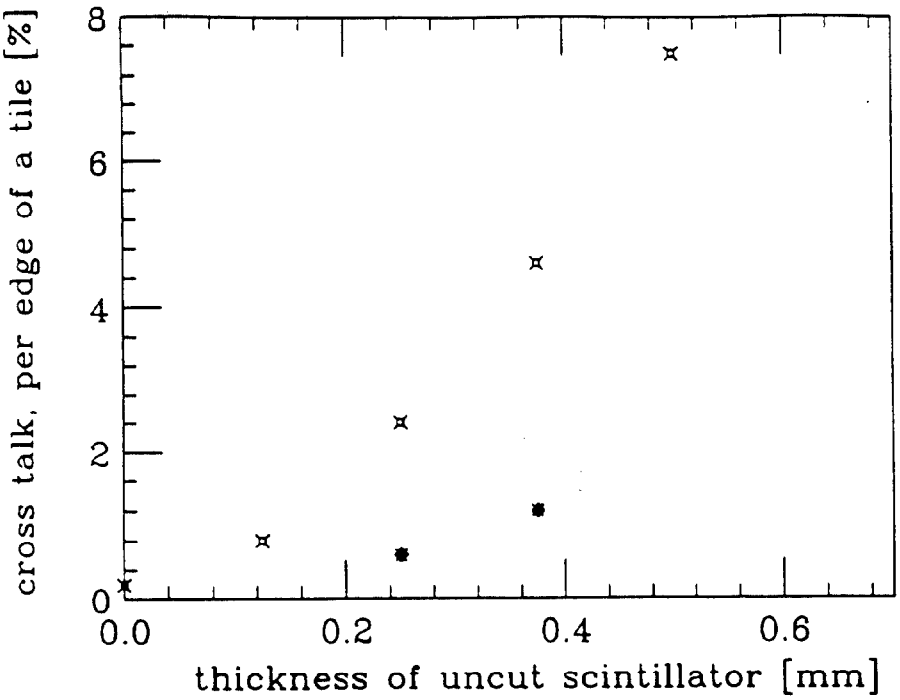

Fig.10: Average light cross-talk between neighbouring tiles, per single edge of a tile, as a function of a depth of an uncut scintillator in the separation groove. Solid data points correspond to the tiles with a black line on the surface of the scintillator between the tiles. Black line reduces the light cross talk to less than 2% level.

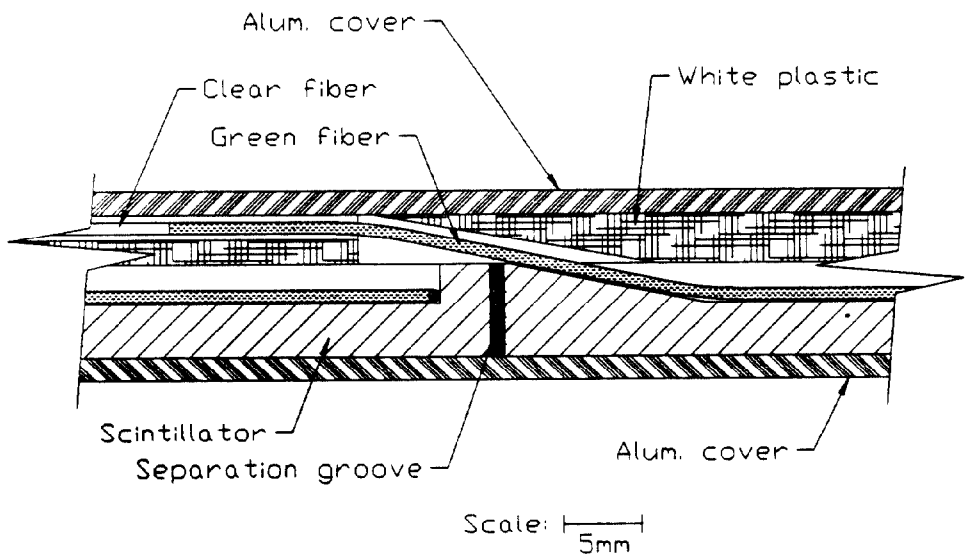

Fig.11: A cross-section of a assembled HAD megatile showing a WLS fiber feeding into the scintillator tile, plastic cover housing clear fibers, and the top and the bottom aluminium covers providing the mechanical protection.

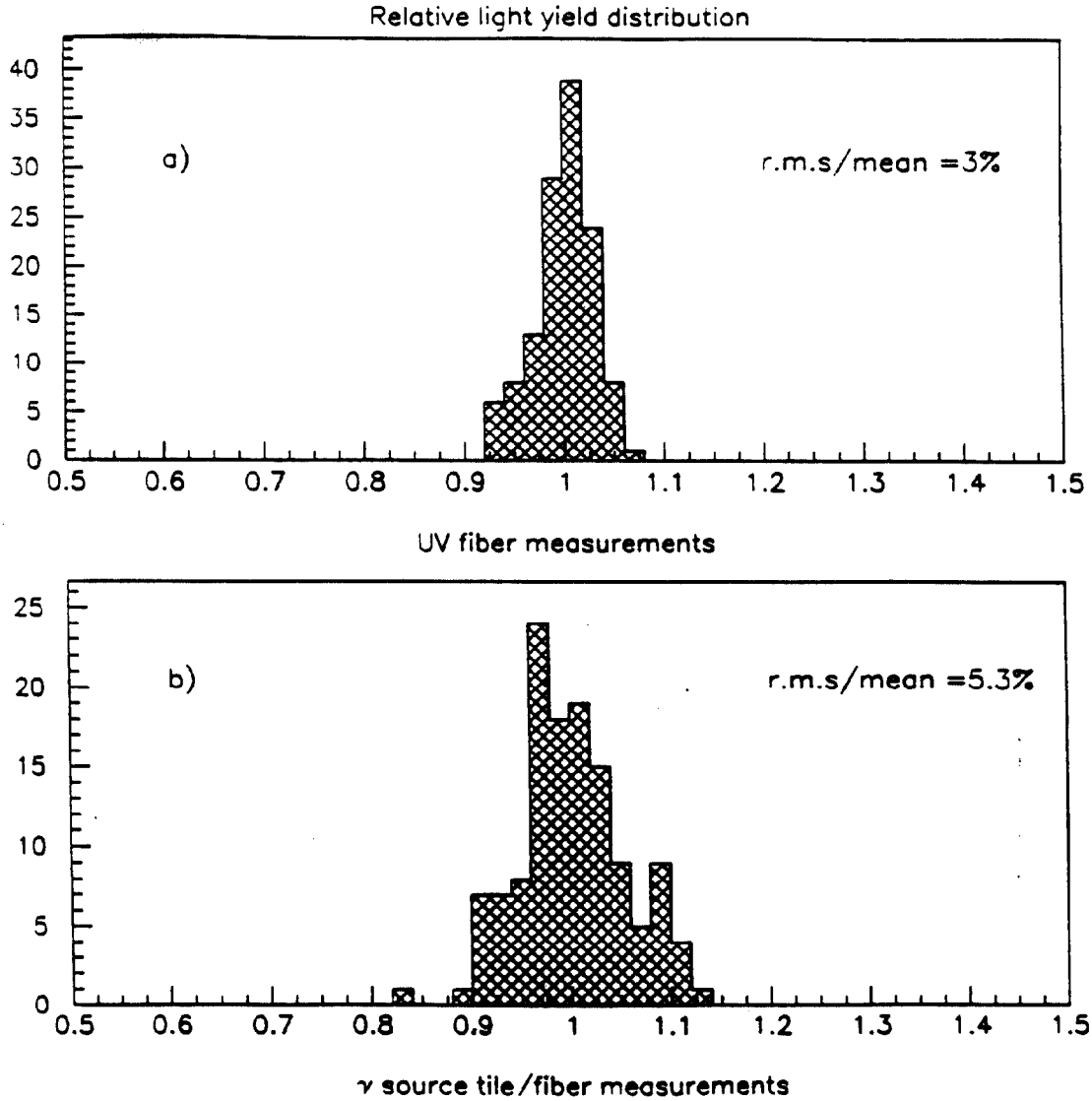

Fig.12: a) Distribution of the relative light yield of fibers from several fiber/connector assemblies before insertion to the megatiles. The r.m.s./mean for this distribution is approximately 3-4%.
b) Distribution of the relative light yield of the tiles from a set of 4 megatiles measured using Cs^{137} γ source scanner. The relative light yield is independently normalized for the groups of tiles from same η regions. The r.m.s./mean is approximately 6%.

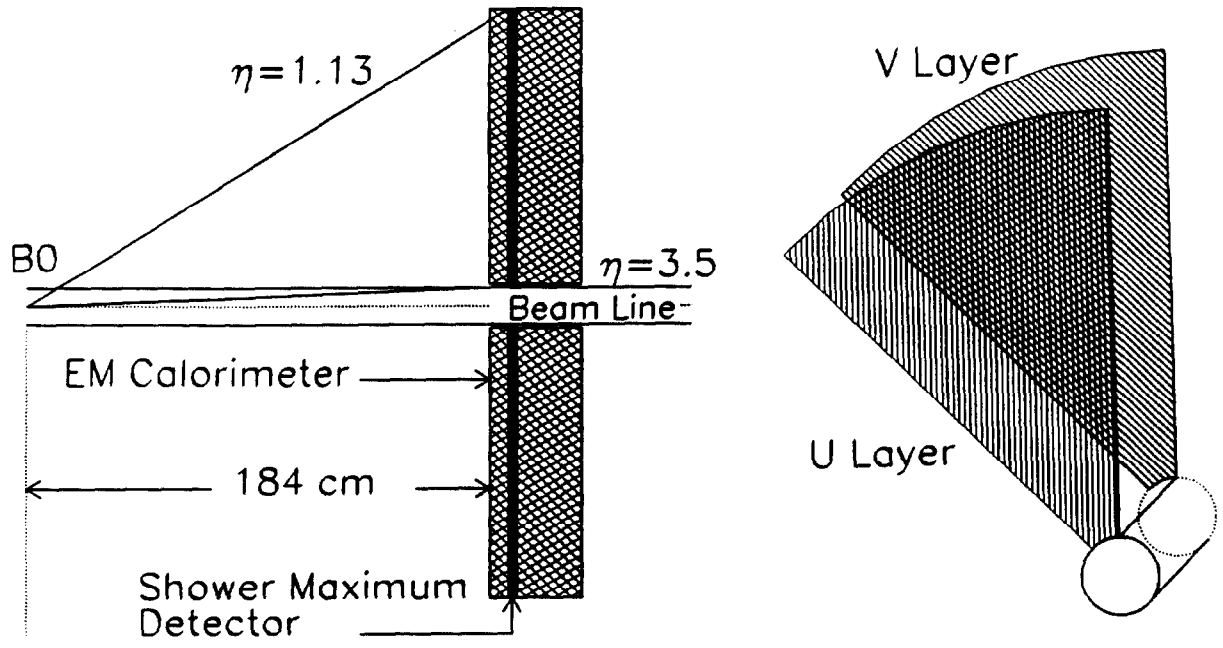

Fig.13: Lateral view of the Shower Maximum Detector (SMD) in the CDF Plug Upgrade (left) and U-V scintillator strips layer in the SMD (right).

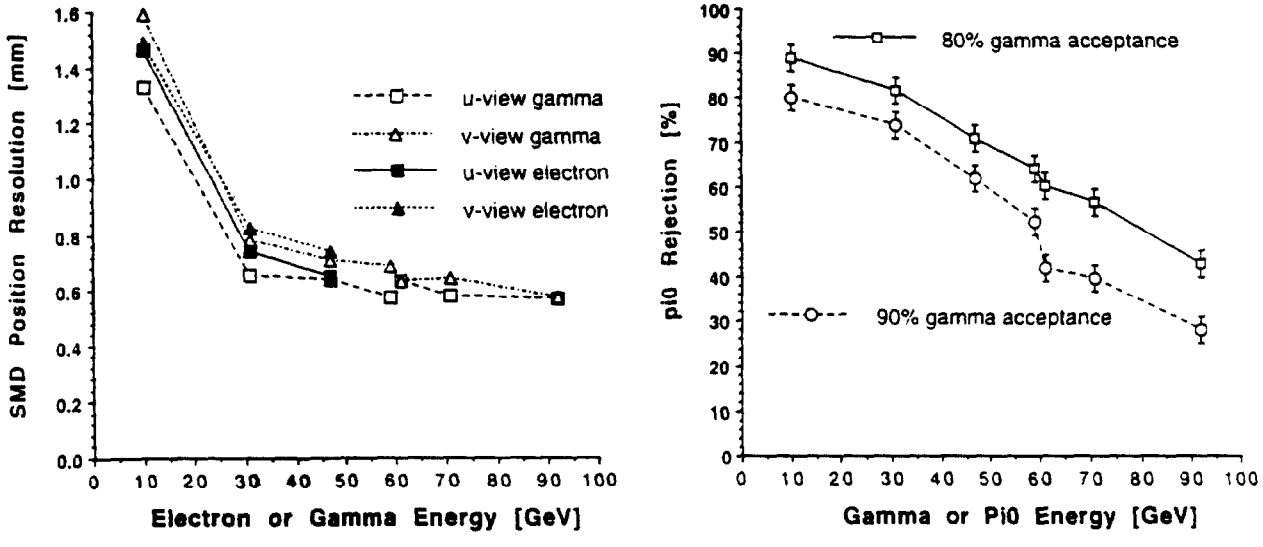

Fig.14: Simulation results for the position resolution and π^0 rejection as a function of energy.

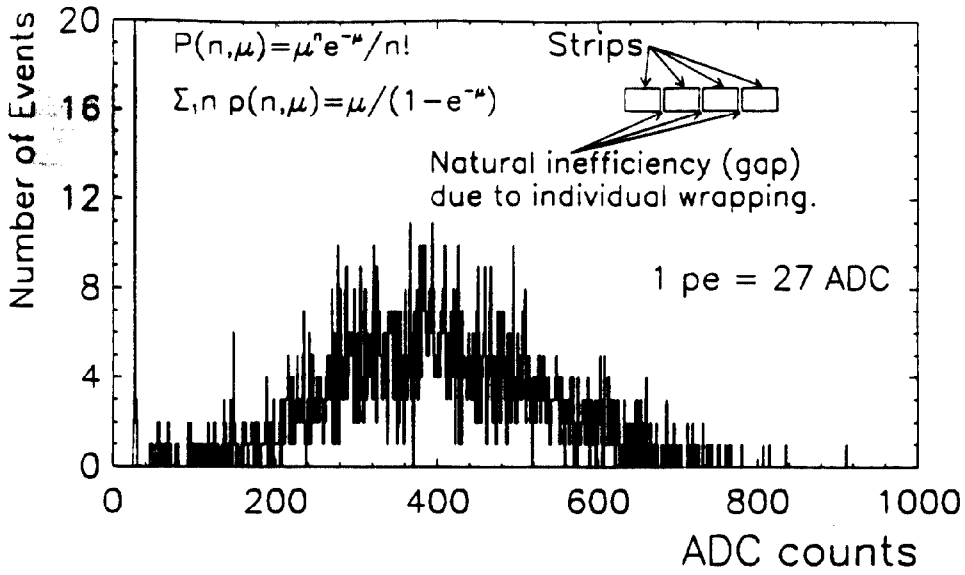

Fig.15: Typical spectral response for the BC404 sample . The standard method to get the number of photoelectrons consists of counting the number of zeros (pedestal counts) and use of the Poisson statistics. Since the setup presents some natural inefficiencies due to the individual strip wrappings and for large light yield these inefficiencies can be larger than the detector inefficiencies, we compute the average of the distribution excluding the zeros. Combining the formula indicated in the figure and the calibration found with a set of reference tiles we get the total number of photoelectrons. A typical calibration value is 1 pe = 27 ADC counts.

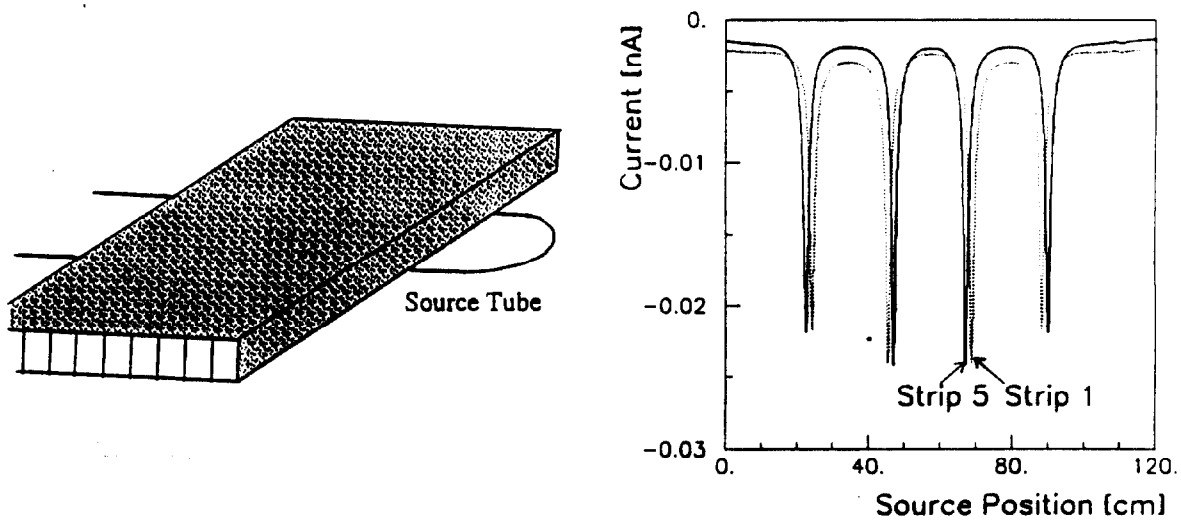

Fig.16: Experimental setup for the calibration scheme test. The different strips are read out by individual standard PMTs (left). Current response for 2 strips (right).

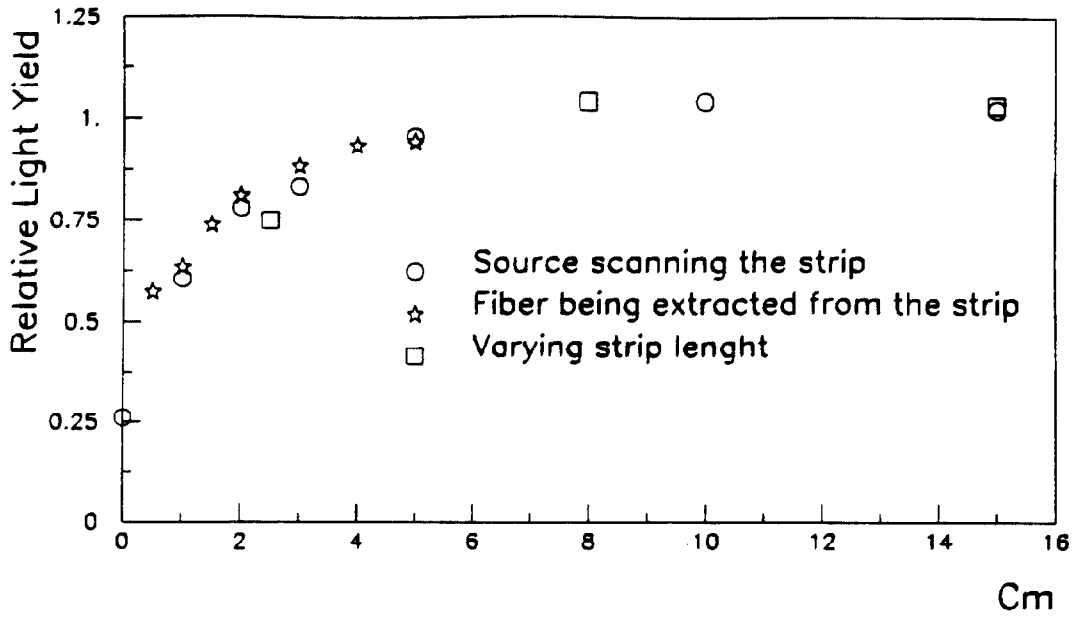

Fig.17: Strip light yield as a function of the strip length.

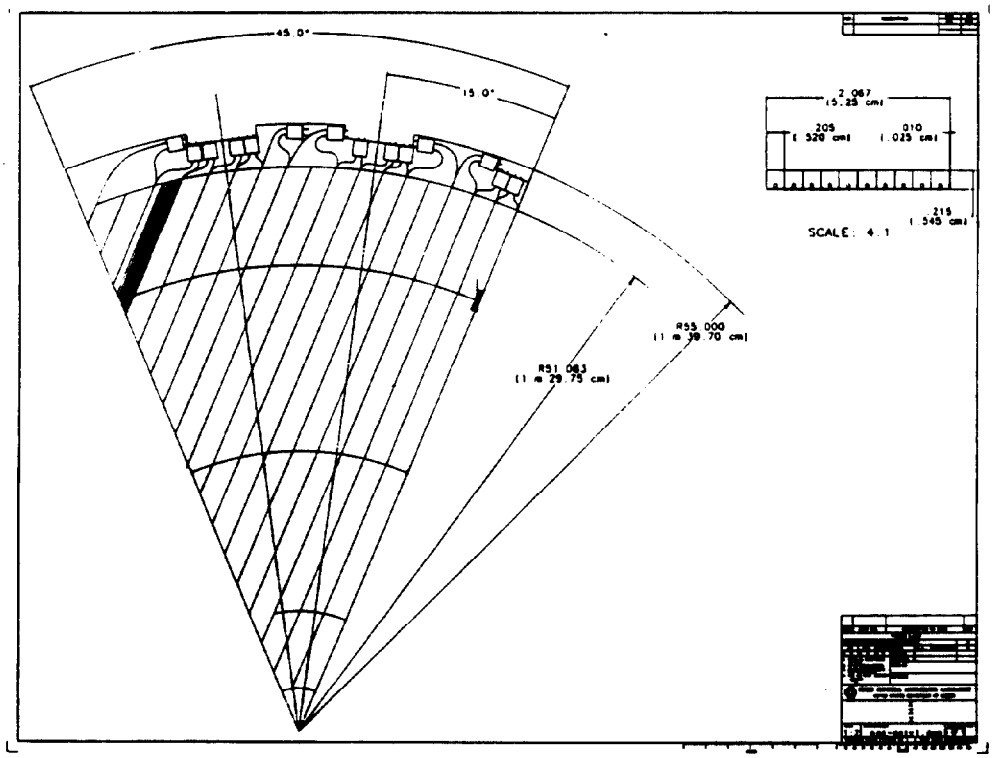

Fig.18: Schematic drawing of one of the two views in a 45^0 sector. All the strips have length greater than 5 cm.

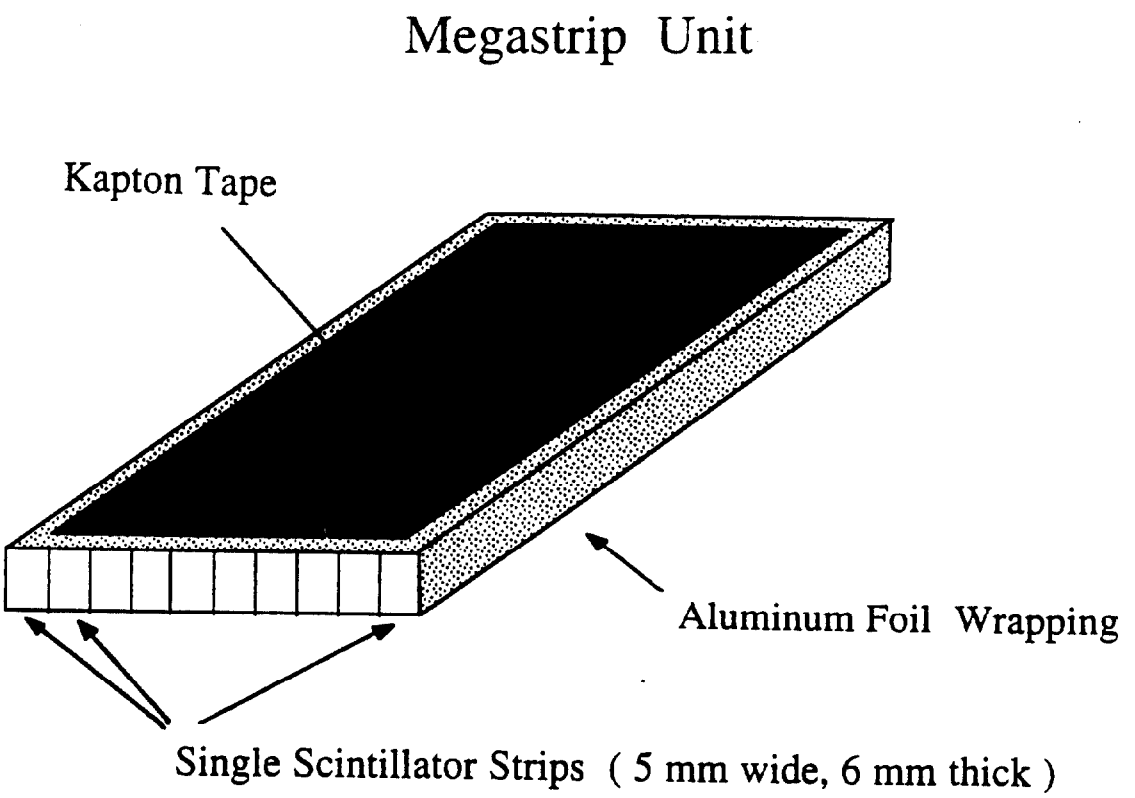

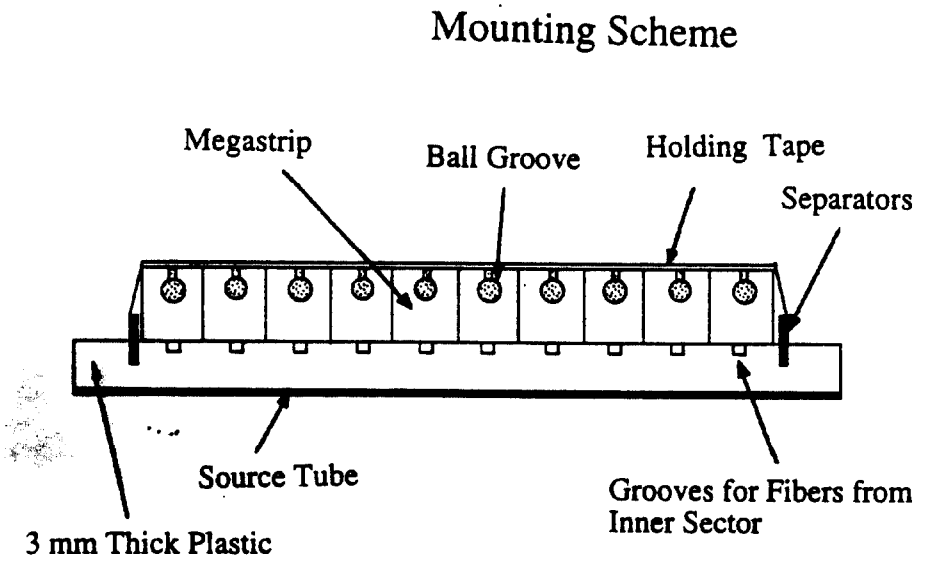

Fig.19: Mounting Scheme for the SMD.